Solid State Phenomena
ISSN: 1662-9779, Vol. 390, pp 75-84
doi:10.4028/p-FSxD8K

Submitted: 2026-01-16
Revised: 2026-02-18
Accepted: 2026-02-20
Online: 2026-04-17

Texture Data Preparation for Finite Element Simulations of Puncture Tests: Insights from the VPSC Approach

Alois C. Ott[1,2,a*], Leo Schwarzmeier[1,b], Johannes Kronsteiner[1,c], Nikolaus P. Papenberg[1,d] and Thomas Antretter[2,e]

[1]LKR Light Metals Technologies, AIT Austrian Institute of Technology, Lamprechtshausener Straße 61, Braunau am Inn / Ranshofen, 5282 Austria

[2]Montanuniversität Leoben, Chair of Mechanics, Franz-Josef Straße 18, Leoben, 8700 Austria

[a]alois.ott@ait.ac.at (*corresponding author), [b]leo.schwarzmeier@ait.ac.at, [c]johannes.kronsteiner@ait.ac.at, [d]nikolaus.papenberg@ait.ac.at, [e]thomas.antretter@unileoben.ac.at

Keywords: Forming, Aluminum Alloy, Anisotropy, Alignment, Clustering, Puncture Test

Abstract. Predicting the deformation behavior of rolled and extruded light metal alloys is a challenging task. Due to the high cost of experimental analysis, finite element simulations are often required. A variety of material models at different scales are available for practical use. In this work, the viscoplastic self-consistent (VPSC) approach is employed to consider microstructural effects. These can be incorporated by using measured crystal sizes and orientations - called texture - of the alloy under consideration. For each integration point in the FE mesh, a corresponding texture is assigned and individually deformed in LS-DYNA®, where VPSC is implemented as a user-defined material model - referred to as FE-VPSC. This study focuses on preprocessing of texture data as well as their compression for accurate and faster FE simulations. For verifying the simulations, a comparison with digital image correlation (DIC) of experimental puncture tests was conducted.

Introduction

The usage of sheet metal alloys in industry is very versatile. A single car is made up of hundreds of individual sheet-metal parts. However, due to construction requirements and the intricacies of the material behavior, complex forming processes with multiple deformation steps are often necessary [1,2,3]. Furthermore, anisotropic behavior of the sheet metal can lead to thinning, cracks or uncontrolled shape deviations during forming [4,5,6]. To understand and thereby mitigate these effects, the simulation of forming processes has gained increasing importance over the past decades. When, in addition, microstructural information is incorporated into the material model, further improvements can be achieved. However, simulations taking into account such a degree of detail are computationally expensive. The viscoplastic self-consistent (VPSC) approach represents a mesoscale material model that provides a viable trade-off between accurately capturing the micromechanical response - including as much information as necessary - and computational cost for a given component size. The microstructural input of the material in our work is derived from electron backscatter diffraction (EBSD) measurements. However, before being used in microstructure simulations [7], this information must be carefully preprocessed.

Sample preparation as well as measurement setup for EBSD analysis often leads to texture misalignment and an excessively large number of grain orientations, which can complicate material simulations. For every sheet metal a physically motivated coordinate system – from here on termed the ‘reference system’ - can be defined, representing the three process directions (rolling-, transversal- and normal direction). The measured grain orientations, i.e. the texture, are expressed by rotation matrices relative to the corresponding measurement coordinate system. To provide optimal material data for simulation, the deviations of the reference system to the measurement system are evaluated and corrected in the preprocessing step. In a second step, grains with almost identical crystallographic orientations are combined by a clustering algorithm specifically adapted for this purpose [8,9]. It has

already been shown, that for sheet metals with a single phase of cubic crystals, 100 grains are more than sufficient to represent the texture [8,9,10].

A practical approach to characterize the material behavior involves puncture tests [11]. Using digital image correlation (DIC) during puncture tests, deformations and cracks of a sheet metal specimen can be detected [12,13]. Moreover, these effects can be replicated through an implementation of VPSC in the finite element framework LS-DYNA® (FE-VPSC). The goal is to use optimized EBSD data to achieve a reasonable agreement with simulation results [14,15,16] at acceptable computational effort.
In the present work, we address these issues by investigating an EN AW-6016-T4 aluminum alloy. For comparison of experiments with simulated puncture tests, the resulting deformation maps are evaluated.

Experimental

For the investigations in this work, an EN AW-6016-T4 sheet metal alloy with a thickness of 1.2 mm was analyzed via EBSD measurements as well as puncture tests.

Texture. For EBSD measurements, a Velocity Super camera of AMETEK/EDAX was employed. The accelerating voltage amounts to 20 kV with a beam intensity of 18, i.e. a unitless Tescan-specific value ranging from 1 to 20. The viewing direction on the sample surface was the plane spanned by the transversal direction (TD) and rolling direction (RD). A working distance of 15 mm was chosen, with a view field of 900 µm and a scanning step size of 1 µm. For data preparation and analysis, the software OIM v8.6 was used. The NPAR clean-up method was employed, using a confidence index (CI) threshold of 0.05. The measured inverse-pole figure (IPF) map as well as the corresponding Pole Figures are provided in Fig. 1.

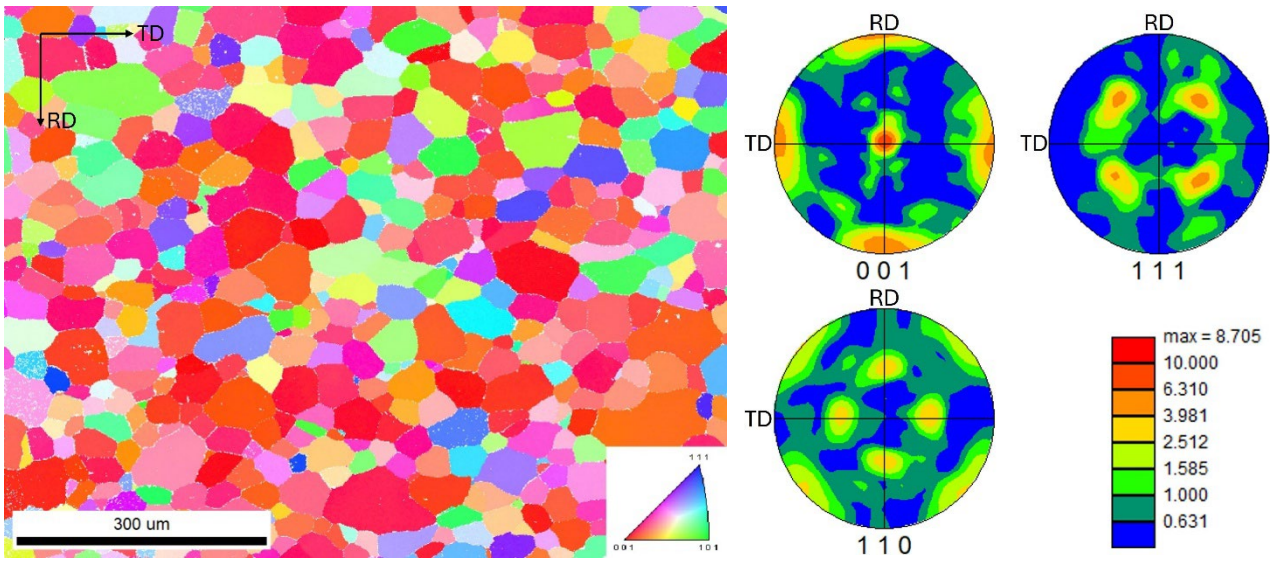

(a) (b)

Fig. 1. Texture measurements of EN AW-6016-T4, showing (a) Inverse Pole Figure map in the [001] crystal direction and (b) the corresponding Pole Figures in the [001], [110], and [111] directions.

Puncture Tests. An electrodynamical testing machine, Linovis (4a Engineering), was employed to perform puncture tests on the chosen sheet metal. In Fig. 2(a) the corresponding test chamber is illustrated. Sheets with dimensions of 80×80 mm were manufactured and painted with white base coat and black speckles. To reduce friction, two layers of Teflon foil coated with bearing grease were applied to the backside. Subsequently, the prepared samples are placed between the two clamping plates and fixed using the two hydraulic cylinders. In a separate chamber on the left side (not visible),

a high-speed camera, FASTCAM NOVA S9, was oriented orthogonal to the sheet surface. The resolution was set to 1024×1024 px with a corresponding view field of 35.84×35.84 mm. The samples were deformed with a speed 0.2 mm/s and ~15 mm deformation path. The movement of the impactor (20 mm diameter) from the right/back side in the chamber led to fracture of the samples, see Fig. 2(b). For determining the optical measured displacements, the software MercuryRT v3.1. was used. Based on the chosen parameter settings, a frame rate of 60 fps was sufficient to ensure accurate DIC measurements.

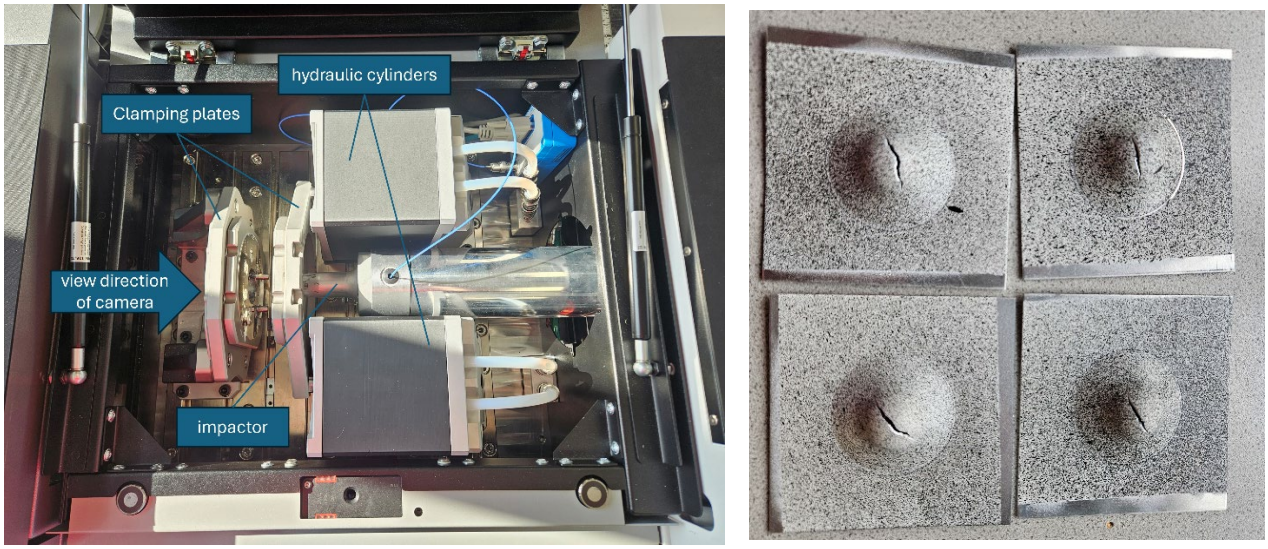

(a) (b)

Fig. 2. Puncture test setup: (a) the Linovis test chamber and (b) samples of four experiments conducted up to fracture.

Methods

To ensure meaningful FE-VPSC simulations, an adequate preprocessing of the texture input data was necessary. Due to sample preparation and positioning of the EBSD detector, the process directions RD, TD and ND did not coincidence with the principal axis of the measurement system. This issue was handled by using an alignment algorithm.
Subsequently, the number of different grain orientations was reduced in order to provide a balanced trade-off between simulation runtime and output quality. For this purpose, a clustering method was applied on the previously aligned texture data.
Finally, the FE setup for conducting puncture simulations is discussed. It includes the VPSC material parameters, the deformation path, the tooling geometry, as well as their combined application in the FE mesh.

Texture Alignment. The texture input for the VPSC material model was derived from EN AW-6016 sheet metal alloy in T4 temper, see IPF map in Fig. 1(a). It was composed almost entirely of grains exhibiting cube orientation, as shown in Fig. 1(b). This is a result of static recrystallization during heat treatment [17,18]. Due to the FCC crystal symmetry as well as orthotropy introduced during the forming process, the grains are symmetrically oriented.
It is known that a symmetrical alignment of the pole figures is equivalent for aligning RD and TD in 2D plane with the two principal axes x and y, see Fig. 3. For the 2D alignment of pole figures we use the division of the upper hemisphere with a grid as shown in Ref. [7]. Following this procedure, the azimuth angle [0°, 360°] and altitude [0, 90°] are divided by 10°, resulting in a grid with 36×9=324 bins. Each bin is assigned the number of poles contained in it. Stereographic projection of the grid onto the equatorial plane yields bins symmetrically distributed along the x- and y-axes, as illustrated in the pole figures of Fig. 3. Since the {111}<110> slip systems are the main contributors for deformation of aluminum at room temperature, the {111} pole figure is afforded special attention

in the alignment process. Through the optimization process described in Ref. [7], the texture gets realigned until the bins in the {111} pole figure are symmetrically aligned with the RD- and TD-axes. This corresponds to the minimal difference of poles in opposing bins. The resulting alignment amounts to an (Euler) angle of 1.91 °. This value is comparatively low, as the texture is sharp and well defined and was therefore already manually aligned with reasonable accuracy during measurement. For less pronounced textures, deviations introduced by the measurement process can reach up to 5 ° [7].

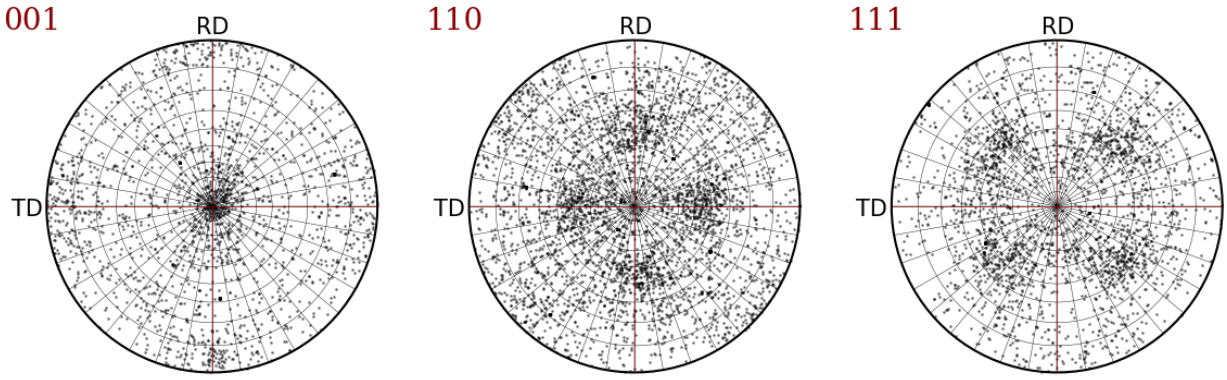

Fig. 3. Pole figures of EN AW-6016-T4 after symmetrical alignment about the RD- and TD-axis of the {111} pole figure.

Texture Clustering. The initial texture of the investigated aluminum sheet consists of 660 grains. From Ref. [8,9,10], it is known that 100 grains are sufficient to describe the orientation distribution function (ODF) of FCC alloys. Since the runtime of VPSC shows a linear relationship with the number of grains used [15], the simulation time of FE-VPSC can be reduced significantly by texture clustering. For this purpose, the clustering algorithm described in Ref. [8,9] is used. It is based on a quaternion representation of each grain and the Euclidean metric defined within this space.

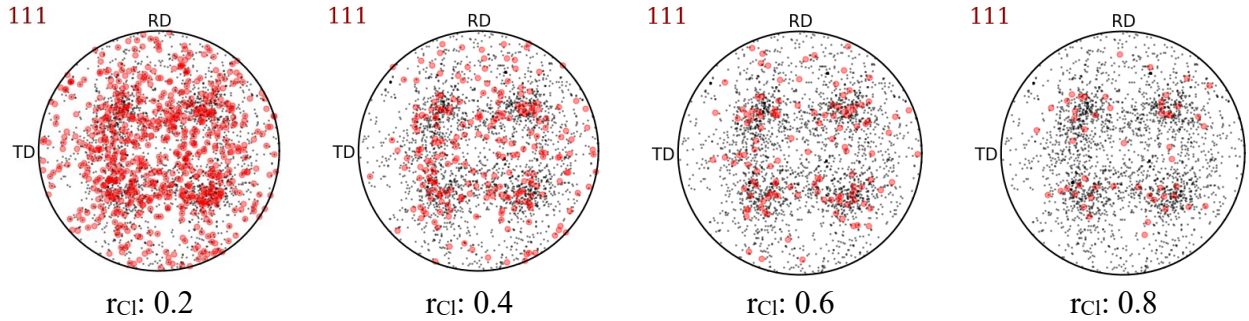

Fig. 4. Comparison of original texture (black) and clustered texture (red) with rising cluster radii (r_{CI}), i.e. increasing texture compression, and reducing number of grains. The cube texture component is preserved through the clustering.

The algorithm starts by assigning each grain to a cluster. The size of a cluster is defined by a radius (r_{CI}) determined from the Euclidean distance to its center. Clusters are then iteratively realigned (with occasional re-creation) until each cluster provides a good average of the grains assigned to it. The dominant texture component, in this case ‘cube’, should be retained as well. This is achieved through the weighted arithmetic mean of the assigned grains, followed by normalization. As shown in Fig. 4 the cube texture component is well preserved for the textures clustered with a r_{CI} of 0.2, 0.4, 0.6 and 0.8. For both tension and compression test simulations, a cluster radius of 0.6 has been shown to provide a good balance between simulation quality and runtime [8,9].

FE-VPSC.
The fundamental principle of the VPSC approach assumes that each individual grain of the considered polycrystalline aggregate possesses an ellipsoidal shape and is embedded in a homogeneous effective medium (HEM). Within a self-consistent framework, the response of all grains is determined such that stress equilibrium and strain compatibility are satisfied in an average sense. This interaction is established through an appropriate linearization scheme. For each individual grain in the polycrystalline aggregate, the continuum relation for the local strain rate $\dot{\boldsymbol{\epsilon}}(\Gamma)$ is given by

$$\dot{\boldsymbol{\epsilon}}(\Gamma) = \dot{\gamma}_0 \sum_{s=1}^{N} \boldsymbol{m}^s(\Gamma) \left(\frac{\boldsymbol{m}^s(\Gamma) : \boldsymbol{\sigma}^c(\Gamma)}{\hat{\tau}^s(\Gamma)} \right)^{\mathrm{n}} \tag{1}$$

Here, $\boldsymbol{m}^s$ denotes the geometric Schmid tensor, $\boldsymbol{\sigma}^c$ the Cauchy stress tensor, and $\hat{\tau}^s$ the critical resolved shear stress after accumulated shear Γ in each grain. The index $s = 1, \ldots, N$ accounts for the different slip systems active in the crystal lattice, while $\dot{\gamma}_0$ represents a reference shear rate.

Furthermore, VPSC is implemented within the LS-DYNA® finite element framework via a user-defined material subroutine (UMAT). Each finite element of the metal sheet is assigned a single integration point governed by the FE-VPSC formulation [19]. At each implicit time step, the deformation increment, and the current texture are passed to the VPSC UMAT, which computes the stress response and updates the local texture accordingly. Further details on the implementation, which is based on an approach developed for the FE solver ABAQUS® [20], can be found in [14,15]. The puncture simulations used the same setup and hardware as described in Ref. [16]. Both the impactor and the die are represented by rigid bodies. Boundary nodes, created to simulate the blank holder, secure the 1.2 mm thick metal sheet. Deformation was realized via the impactor, which moved with a constant velocity of 0.1 mm/s. A standard friction coefficient for aluminum-steel contact at room temperature was applied to define the interactions between the impactor and the metal sheet, as well as the sheet and the die, see Fig. 5. It should be noted that this definition of interaction differs from the experimental setup, where Teflon and lubrication were employed to minimize friction between the impactor and the sheet metal.

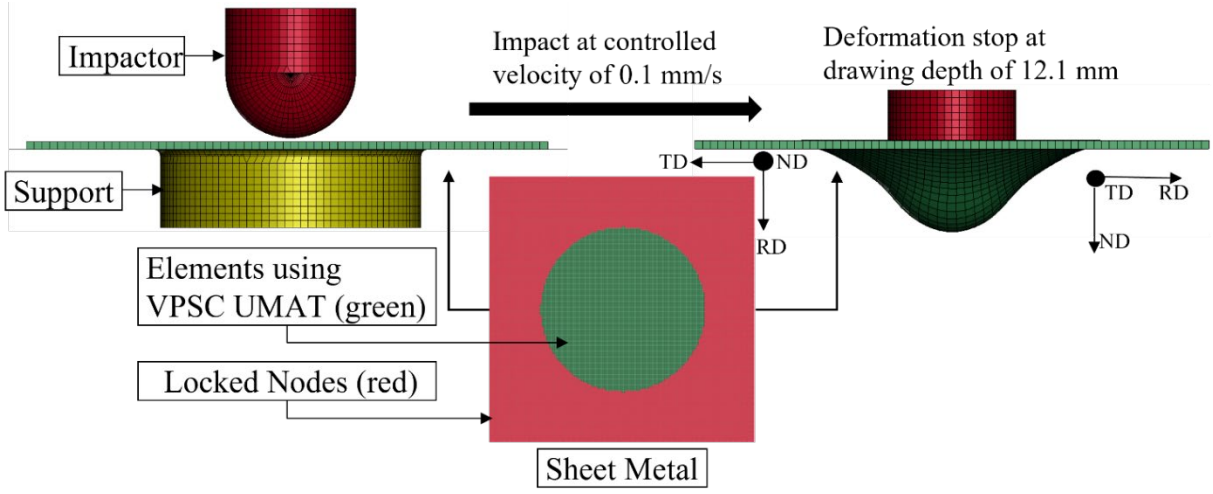

Fig. 5. Overview of the FE meshes used in the LS-DYNA® puncture test simulations. VPSC was implemented as a UMAT for the part representing the metal sheet specimen, which comprised approximately 4.4k elements. The impactor, with a diameter of 20 mm, and the die featuring a 40 mm opening were modelled as rigid bodies, representing the steel components of the experimental setup.

The employed VPSC material model was restricted to the {111}<110> slip system, as face-centered cubic (fcc) materials deform predominantly by slip on this system at room temperature [4]. The associated self-hardening behavior was described using the (extended) Voce hardening law, whereby the evolution of the critical resolved shear stress (CRSS) of the slip system is given by

$$\hat{\tau}^s(\Gamma) = \tau_0 + (\tau_1 + \theta_1\Gamma)\left[1 - exp\left(-\Gamma\left|\frac{\theta_0}{\tau_1}\right|\right)\right]. \quad (2)$$

Here, Γ denotes the accumulated total shear stress within the grain, while τ_0, τ_1, θ_0 and θ_1 represent the Voce hardening parameters. Although VPSC enables the incorporation of latent hardening effects, these were neglected in the present study, as only a single slip system was considered.
The Voce hardening parameters in Equation (2) were taken from Ref. [16], which investigated the same material. Specifically, the flow curve obtained from an experimental tensile test of EN AW-6016-T4 in the rolling direction (RD) was calibrated using LS-OPT (v. 7.0.2). The calibration was performed by systematically varying the hardening parameters within an FE-VPSC simulation of the tensile specimen geometry until agreement with the experimental response was achieved.
The resulting Voce parameters τ_0=66.18 MPa, τ_1=68.56 MPa, θ_0=423.28 MPa, θ_1=0 MPa, are adopted throughout this study. The N-effective linearization scheme was applied with an interaction parameter n_{eff}=10.

Results and Discussion

This section examines the effects of texture alignment and varying degrees of texture clustering on the FE-VPSC simulations of puncture tests. The simulation results show good agreement with the experimental observations.

Texture Alignment. The measured texture of EN AW-6016-T4, with and without automated alignment, is shown in Fig. 1(b) and Fig. 3, respectively. Both textures were subsequently clustered using a cluster radius of 0.4. The resulting clustered textures serve as input for the FE-VPSC puncture simulations, see Fig. 6.

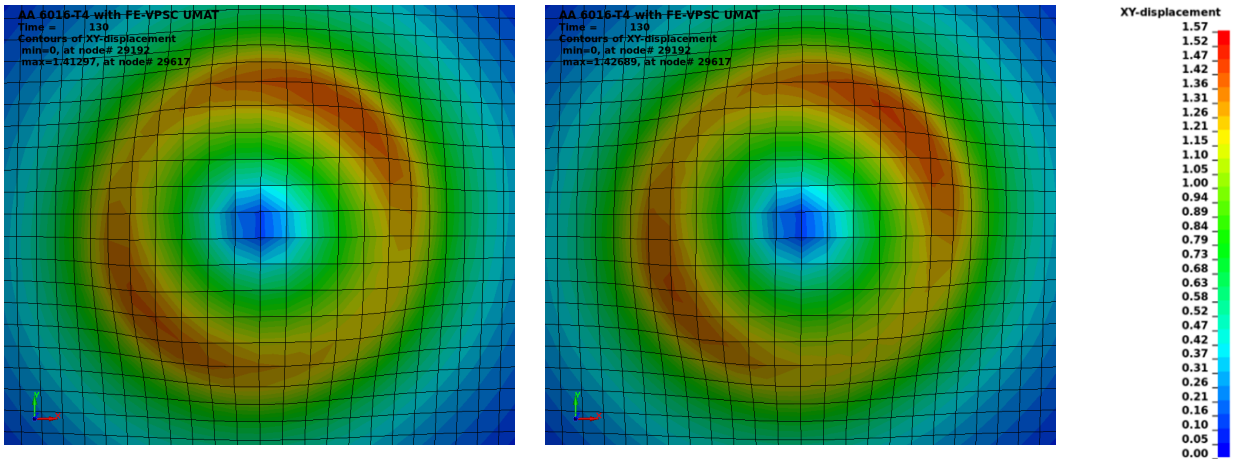

(a) (b) unit in mm

Fig. 6. Results of FE-VPSC puncture simulations, comparing XY-displacement of (a) measured, i.e. manually aligned, texture and (b) and automatically aligned texture.

Small differences are visible by comparing the resulting displacement maps after performing both simulations. The angular position of the two resulting maxima obtained from the manually aligned texture input deviates from the results obtained from the automatically aligned texture input by an offset angle of about 10 °, even though the misalignment between manually and automatically aligned texture only amounts to ~2 °. It appears that even minor variations in the texture can strongly affect the puncture test simulations. The maximum value of deformation in the manual case is 1.413 mm in comparison to 1.427 mm for the automatically aligned case.

Texture Clustering. The influence of four texture clustering levels on the FE-VPSC puncture simulations is investigated. Fig. 7(a)-(d) shows the corresponding XY-displacement maps obtained using input textures of EN AW-6016-T4 with cluster radii 0.2, 0.4, 0.6 and 0.8, respectively. An overview of the results is given in Table 1.

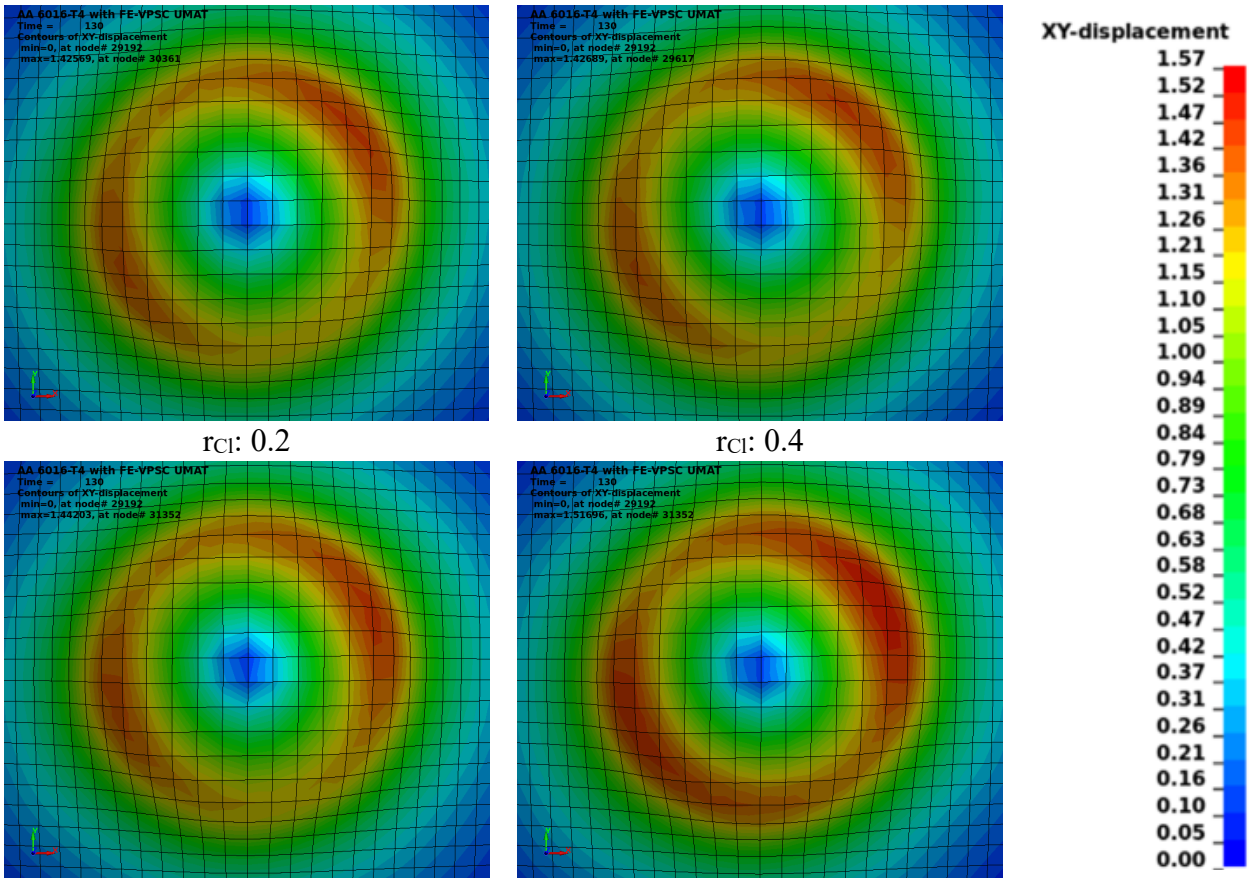

Fig. 7. Resulting XY-displacement of simulated puncture tests via FE-VPSC, using four clustered textures, cluster radii (r_{CI}) 0.2 to 0.8, as input.

Between the input textures with cluster radii of 0.2 and 0.4 only minor deviations in the locations of the two resulting maxima fields can be observed. Accordingly, the maximum deformation changes marginally, from 1.426 mm to 1.427 mm. For a cluster radius of 0.6 more pronounced deviations in the localization of the deformation maxima become apparent, and the maximum displacement increases to 1.442 mm. The deformation map obtained with a cluster radius 0.8 exhibits clear visual differences, with peak values reaching 1.517 mm.

Table 1. Characteristics of simulated puncture tests with varying degrees of input texture clustering.

Cluster Radius	Number of Clusters	XY-Displacement Maximum	Runtime FE-VPSC
0.2	167	1.426 mm	37h 11min 35s
0.4	57	1.427 mm	19h 55min 11s
0.6	30	1.442 mm	13h 44min 50s
0.8	13	1.517 mm	10h 18min 44s

Regarding computational runtime, the simulation using a cluster radius of 0.2 required 37h 11min 35s. Compared to the original texture consisting of 660 grains, the reduced texture obtained with a cluster radius of 0.2 consists of 167 clusters. Increasing r_{CI} from 0.2 to 0.4 results in an approximate reduction in the number of grains by two thirds i.e. to 57 grains, which corresponds to a runtime reduction of roughly 50% down to 19h 55min 11s. In contrast, clustering with a radius of 0.6 reduces the texture further to 30 grains and yields a runtime as low as 13h 44min 50s. However, this level of data reduction already leads to considerable differences in the simulation results, i.e. in the maximum XY-displacement. The cluster radius of 0.8 reduces the texture to 13 grains but results in only a limited further reduction of the runtime to 10h 18min 44s. It can also be observed that the reduction in computation time is no longer proportional to the number of grains, indicating that solver overhead becomes significant at this level of clustering.

Experimental validation. Based on the presented results, a cluster radius of 0.4 appears to represent the optimal trade-off between accuracy and computational efficiency. For tensile- and compression simulations with FE-VPSC [8,9] even a higher clustering radius of 0.6 was adequate. To verify the FE-VPSC puncture test simulations, a comparison is made with the experimental deformation maps from DIC measurements. To obviate the influence of static friction on the metal sheet surface, the deformation maps are evaluated with an applied puncture force of approximately 1300 N. The resulting deformation maps of the four conducted experiments are shown in Fig. 8. For enhanced visualization, the upper bound of the color scale was capped at 0.20 mm, the maxima exceeding this value are displayed in white. Consequently, it is now evident that the maxima develop with an offset of approximately 45 ° relative to the principal axes. This behavior was expected due to the high fraction of cube texture component and the presence of in-plane shear [21]. This effect is even more pronounced in the puncture simulations at higher forces, which shows good agreement with the experimental observations.

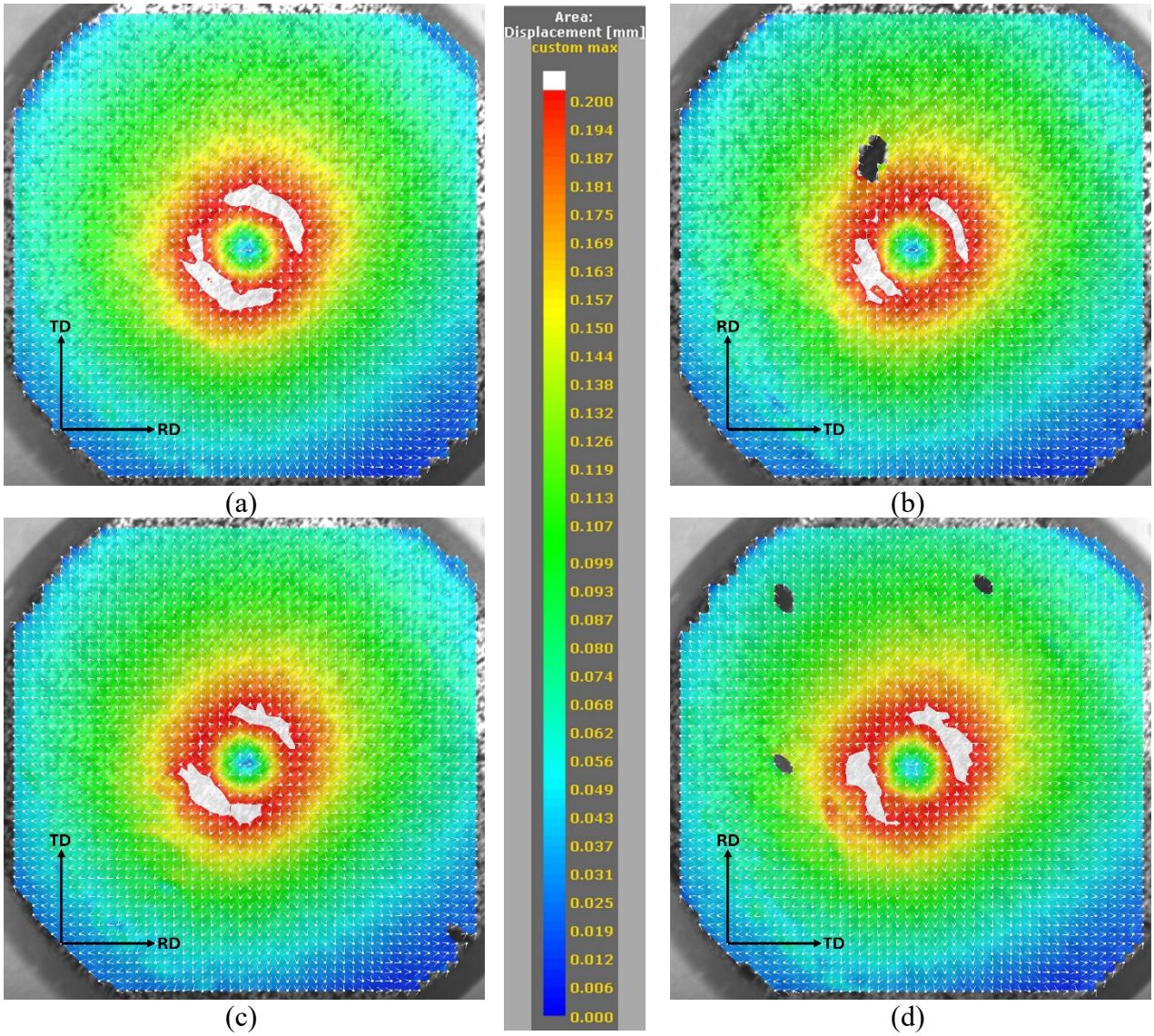

Fig. 8. Displacement maps from four experimentally conducted puncture tests performed at deformation forces of approximately 1300 N are presented. For improved visualization, the upper limit of the color scale was capped at 0.20 mm; deformation values exceeding this threshold are displayed in white. This adjustment highlights the consistent formation of two maxima regions, offset by 45°, across all tests. In Figures 8(b) and 8(d), localized voids appear in the displacement field. These result from oversized speckles on the specimen surface that could not be reliably captured during digital image correlation (DIC) analysis.

Summary

The puncture test simulations performed with FE-VPSC exhibit good agreement with the experimental DIC results regarding the (RD,TD)-displacement. Anisotropic effects, particularly at 45 ° between the rolling direction (RD) and transverse direction (TD), are clearly visible in the (RD,TD)-displacement field.
These results were achieved by processing the original texture to align the measurement coordinate system with the manufacturing directions. This involves an adjustment of approximately 2° which already induced non-negligible changes in the simulation results. In a second step, an efficient data reduction was applied using a clustering algorithm tailored for grain orientation data. A cluster radius of 0.4 provided a favorable balance between accuracy and computational efficiency.

Acknowledgement

This research has been funded by the Fonds Zukunft Österreich within the framework “Industrienahe Dissertationen 2025” in the project “MaLTe” administered by FFG under the grant number FO999926074 and by the project “Data-T-Rex” (Wi-2021-305676/13-Au) which is cofinanced by research subsidies granted by the government of Upper Austria. The authors would also like to thank Los Alamos National Laboratory, and especially Miroslav Zecevic, for providing the FE-VPSC code.

References

[1] D. De Cupis, H. de Carvalho Pinheiro, A. Ferraris, A.G. Airale, M. Carello, Active aerodynamics design methodology for vehicle dynamics enhancement, in: Proceedings of the International Conference of IFToMM ITALY, Springer International Publishing, Cham, 2020, pp. 777–785.

[2] Y. Fujii, M. Urabe, Y. Yamasaki, Y. Tamai, Development of press-forming technique for bent automotive body parts using in-plane shear deformation, Mater. Trans. 63 (2022) 622–628.

[3] E. Evin, M. Tomáš, The selection of materials for the auto-body deformation zones, in: Materials Science Forum, Vol. 994, Trans Tech Publications Ltd., 2020, pp. 44–51.

[4] O. Engler, Correlating crystallographic texture with anisotropic properties and sheet metal forming of aluminium alloys, J. Mater. Res. Technol. 35 (2025) 514–522.

[5] W.F. Hosford, Influence of textures on sheet forming, SAE Technical Paper, 2000.

[6] A.K. Addis, Automobile roof panel forming: prediction and compensation of springback and application of numerical simulation based on dynaform, World J. Eng. Technol. 6 (2018) 914.

[7] A.C. Ott, I. Weißensteiner, A.R. Arnoldt, J.A. Österreicher, N.P. Papenberg, Automatic texture alignment by optimization method, Microsc. Microanal. 30 (2024) 253–277.

[8] A.C. Ott, J. Kronsteiner, L. Schwarzmeier, E. Theil, A.R. Arnoldt, N.P. Papenberg, Evaluation of a clustering algorithm for texture data, Mater. Charact. (2025) 115122.

[9] A.C. Ott, E. Theil, J. Kronsteiner, N.P. Papenberg, Introduction of a clustering algorithm evaluated via the texture input of VPSC computations, Results Mater. (2025) 100806.

[10] R.E. Marki, M. Knezevic, Nonlinear optimization for compact representation of orientation distributions based on generalized spherical harmonics, J. Mech. Phys. Solids 187 (2024) 105609.

[11] E. Corona, M. Spletzer, B.T. Lester, C.J. Fietek, Validation of material models for puncture of 7075-T651 aluminum plate, Int. J. Solids Struct. 257 (2022) 111893.

[12] M. Schwab, S. Riemelmoser, Automated evaluation of forming limit curves using 3D-DIC and LINOVIS for sheet metal forming simulations, presented at the International LS-DYNA Conference, Munich, Germany, 28–30 Oct. 2025.

[13] A. Hijazi, N. Yardi, V. Madhavan, Determination of forming limit curves using 3D digital image correlation and in-situ observation, in: Proceedings of SAMPE, 2004, pp. 16–20.

[14] J. Kronsteiner, E. Theil, A.C. Ott, A.R. Arnoldt, N.P. Papenberg, Modeling of texture development during metal forming using finite element visco-plastic self-consistent model, Crystals 14 (2024) 533.

[15] J. Kronsteiner, A.C. Ott, L.O. Felder, L. Schwarzmeier, N.P. Papenberg, Integrating texture evolution into a deep-drawing simulation via viscoplastic self-consistent model, Mater. Charact. 224 (2025) 114970.

[16] L. Schwarzmeier, N. Papenberg, A.C. Ott, J. Kronsteiner, Multiscale modelling of metal anisotropy using the viscoplastic self-consistent (VPSC) approach as a user-defined material model (UMAT) within LS-DYNA, in: Proceedings of the 2025 EMEA Ansys Transportation Summit and International LS-DYNA Conference, Ansys Inc., 2025.

[17] J. Hirsch, O. Engler, Texture, local orientation and microstructure in industrial Al-alloys, in: Proceedings of the 16th Risø International Symposium, 1995, pp. 49–62.

[18] D.N. Lee, H.N. Han, The cube recrystallization-texture related component in the β-fiber rolling-texture FCC metals, in: Materials Science Forum, Vol. 783, Trans Tech Publications Ltd., 2014, pp. 51–56.

[19] J. Segurado, R.A. Lebensohn, J. LLorca, C.N. Tomé, Multiscale modeling of plasticity based on embedding the viscoplastic self-consistent formulation in implicit finite elements, Int. J. Plasticity 28 (2012) 124–140.

[20] M. Zecevic, M. Knezevic, A new visco-plastic self-consistent formulation implicit in dislocation-based hardening within implicit finite elements: Application to high strain rate and impact deformation of tantalum, Comput. Methods Appl. Mech. Eng. 341 (2018) 888–916.

[21] M.A. Bertinetti, C.D. Schwindt, J.W. Signorelli, Effect of the cube orientation on formability for FCC materials: A detailed comparison between full-constraint and self-consisten predictions, Int. J. Mech. Sci. 87 (2014) 200-217.